Neuron
Report

Millisecond-Timescale Optical Control of Neural Dynamics in the Nonhuman Primate Brain

Xue Han,[1,*] Xiaofeng Qian,[1] Jacob G. Bernstein,[1] Hui-hui Zhou,[2] Giovanni Talei Franzesi,[1] Patrick Stern,[3] Roderick T. Bronson,[3] Ann M. Graybiel,[2] Robert Desimone,[2] and Edward S. Boyden[1,2,4,*]
[1]Media Lab, Synthetic Neurobiology Group
[2]McGovern Institute, Department of Brain and Cognitive Sciences
[3]Koch Center for Cancer Research
[4]Department of Biological Engineering
Massachusetts Institute of Technology, 77 Massachusetts Avenue, Cambridge, MA 02139, USA
*Correspondence: xuehan1@gmail.com (X.H.), esb@media.mit.edu (E.S.B.)
DOI 10.1016/j.neuron.2009.03.011

SUMMARY

To understand how brain states and behaviors are generated by neural circuits, it would be useful to be able to perturb precisely the activity of specific cell types and pathways in the nonhuman primate nervous system. We used lentivirus to target the light-activated cation channel channelrhodopsin-2 (ChR2) specifically to excitatory neurons of the macaque frontal cortex. Using a laser-coupled optical fiber in conjunction with a recording microelectrode, we showed that activation of excitatory neurons resulted in well-timed excitatory and suppressive influences on neocortical neural networks. ChR2 was safely expressed, and could mediate optical neuromodulation, in primate neocortex over many months. These findings highlight a methodology for investigating the causal role of specific cell types in nonhuman primate neural computation, cognition, and behavior, and open up the possibility of a new generation of ultraprecise neurological and psychiatric therapeutics via cell-type-specific optical neural control prosthetics.

INTRODUCTION

The rhesus macaque is an important model species for understanding neural computation, cognition, and behavior, as well as for probing the circuit-level basis of human neurological and psychiatric disorders. To resolve how complex functions emerge from the activity of diverse cell types, ideally one would be able to perturb the activity of genetically specified cell types and neural pathways in the primate brain, in a temporally precise fashion. In one recent study, adeno-associated virus (AAV) was used to deliver the *Drosophila* allatostatin receptor to neurons in the primate thalamus (Tan et al., 2006), enabling neural silencing via intracranial delivery of the small molecule allatostatin. In general, however, the adaptation of neural control tools to the primate brain has been slow in comparison to the rapid adaptation of such tools for characterizing circuit functions in worms, flies, and mice (reviewed in Luo et al., 2008). Indeed, although molecular techniques have been used to deliver genetic payloads to the primate brain (e.g., Kordower et al., 2000; Liu et al., 2004; Stettler et al., 2006), as well as to make transgenic primates (Chan et al., 2001; Yang et al., 2008), no attempts have been made to target genes to genetically specified neuron types. Here we used channelrhodopsin-2 (ChR2), a genetically encoded molecular sensitizer that enables activation of neurons in response to pulses of blue light (Boyden et al., 2005; Han and Boyden, 2007; Ishizuka et al., 2006; Li et al., 2005; Nagel et al., 2003; Zhang et al., 2007), to assess the impact of selective activation of cortical excitatory neurons on primate cortical dynamics. We used optical fibers in conjunction with microelectrodes to perform simultaneous in vivo optical stimulation and electrical recording in the awake primate. Selectively activating ChR2-positive excitatory neurons resulted in well-timed excitatory and suppressive influences on neural activity, reflecting neural dynamics downstream of excitatory neuron activation. ChR2 was safely expressed and could mediate temporally precise optical neural stimulation of significant volumes of cortical tissue for months after viral injection, opening up the possibility for such technologies to support precise, cell-specific optical control prosthetics for patients with severe neurological and psychiatric disorders.

RESULTS

We targeted ChR2-GFP to neurons in the frontal cortex in two monkeys (denoted N and A), by injecting VSVg-pseudotyped lentivirus carrying the ChR2-GFP gene behind the 1.3 kb α-CaMKII promoter (Figure 1A; details in Supplemental Experimental Procedures, available online), as used before in mice to target excitatory neurons (Dittgen et al., 2004). To insure repeatable targeting of viruses, optical fibers, and electrodes to the same sites over extended periods of time (Figure 1B), we designed and used a grid to coordinate stereotactic virus injections, photostimulation, and recording (Figure 1C). Histology showed that 1 μl viral injections labeled roughly spherical regions of cortex 1.4 ± 0.5 mm in diameter (mean ± standard deviation [SD]; exemplar in Figure 1D; details in Figure S4, available online). We did not observe GFP-positive cells in thalamic regions that project to injected regions, indicating a lack of retrograde labeling using lentivirus prepared as described. ChR2-GFP appeared to be

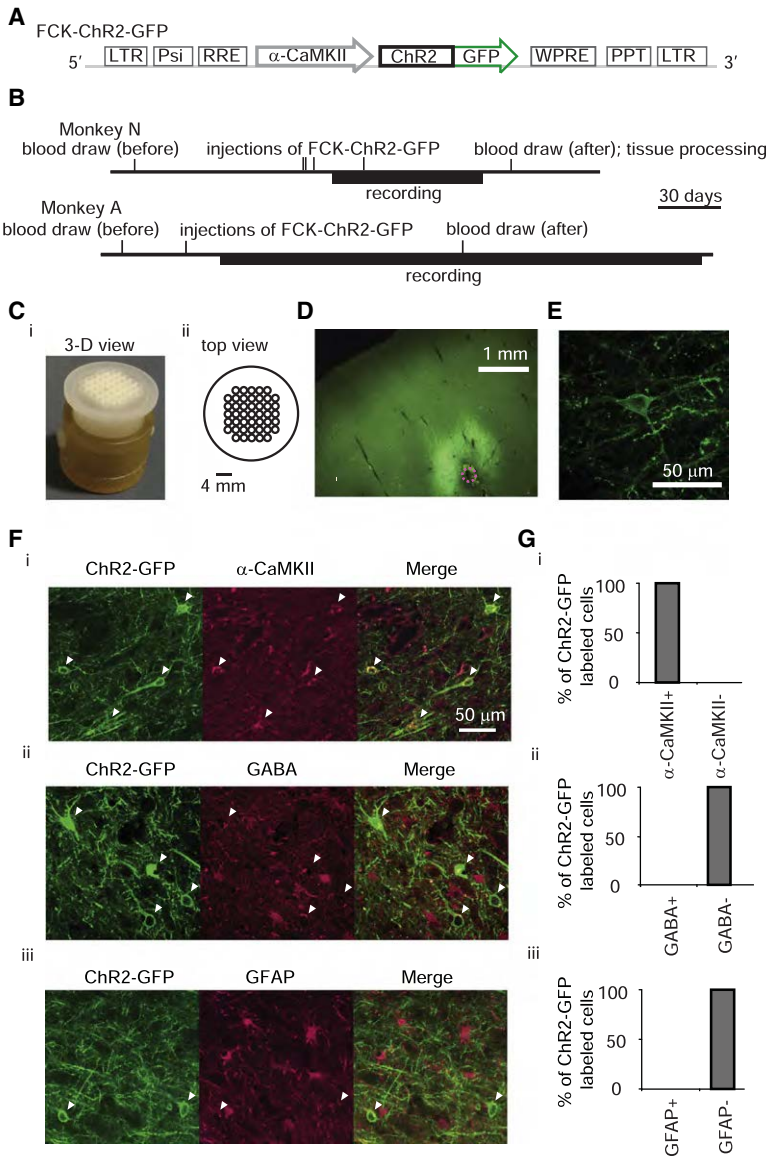

Figure 1. Expression of ChR2-GFP in Excitatory Neurons in Frontal Cortex of Primate Brain

(A) Schematic of lentiviral cassette. (B) Timeline of experiments for monkey N (top) and monkey A (bottom). (C) 3D printed targeting grid, inserted into a recording chamber (Ci) and in a top-view schematic (Cii). (D) Fluorescence image showing ChR2-GFP expression in deep layers of cortex (coronal slice; dotted magenta circle indicates diameter of virus injection cannula). (E) Representative cortical neuron expressing ChR2-GFP. (F) Images of anti-GFP fluorescence (left) as well as immunofluorescence of three cell-type markers: α-CaMKII (Fi), GABA (Fii), and GFAP (Fiii) (middle; right, overlay of the two left images). Arrowheads indicate ChR2-GFP-positive cell bodies. (G) Percent of ChR2-GFP-positive cells coexpressing each of the three markers in (F).

well localized to the plasma membrane at the cell body and throughout neuronal processes (Figure 1E). To assess the cell-type specificity of ChR2-GFP gene expression driven by the α-CaMKII promoter, we immunostained primate cortical slices with antibodies against the excitatory neuron-specific marker α-CaMKII (Jones et al., 1994; Tighilet et al., 1998), the inhibitory neuron-specific neurotransmitter GABA (Hendry et al., 1989; Houser et al., 1983), and the astrocyte-specific marker glial fibrillary acidic protein (GFAP) (Cahoy et al., 2008; McLendon and Bigner, 1994). Neurons expressing ChR2-GFP were positive for α-CaMKII (Figure 1Fi), but not GABA (Figure 1Fii) or GFAP (Figure 1Fiii). Of the ChR2-GFP-positive neurons examined, all coexpressed α-CaMKII (127/127 cells; Figure 1Gi), but none coexpressed GABA (Figure 1Gii, 0/78 cells) or GFAP (Figure 1Giii, 0/84 cells). In order to gauge the efficiency of viral labeling, we counted the fraction of α-CaMKII-positive cells that expressed ChR2-GFP. Near centers of injection sites, where ChR2-GFP expression peaked, 78% ± 8% of the α-CaMKII-positive cells expressed ChR2-GFP (mean ± SD; n = 3 fields of view; 42 ChR2-GFP neurons counted). Thus, lentivirus expressing ChR2-GFP under the α-CaMKII promoter enables cell-specific targeting and efficient expression of ChR2-GFP in excitatory neurons of the monkey frontal cortex.

Given the extended duration of nonhuman primate experiments, and the prospect of using cell-specific optical neuroprosthetics for therapy, we assessed the safety of ChR2-GFP expression in primate brain. After months of ChR2-GFP expression, during which time we repeatedly illuminated neurons with blue light and successfully made recordings, we saw widespread expression of ChR2-GFP in healthy-looking neurons, with no histological abnormalities in neurons or glia, and no immune reaction at the cellular or antibody level (Figure 2; see detailed text in Supplemental Data). These multiple lines of evidence together support the safety of ChR2-GFP expression in the brain of the nonhuman primate, and if supported by further and longer-term analyses, may provide the basis for cell-specific neuromodulation therapy in humans.

To assess the effect of optical activation of ChR2-expressing excitatory neurons on frontal cortical neural circuits in awake monkey, we developed a system appropriate for in vivo monkey use, coupling a fiber to a blue 473 nm laser (Bernstein et al., 2008) and assembling multiple electrodes into independently controlled drives (Figures 3Ai and 3Aii), which were then inserted into a single hole within the 3D printed grid (Figure 1C). This setup allowed us to record from neurons while exposing local cortex to pulses of blue light. In regions of cortex that were not virus labeled, we never observed light modulation of neural activity (n = 32 such sites). In regions that were virus labeled, many neurons increased their firing rate during cortical exposure to blue light (Figures 3B and 3C). We called these neurons "excited" units. In addition to these excited units, many neurons decreased their firing rate during cortical exposure to blue light (Figures 3D and 3E). We called these neurons "suppressed" units, because they did not increase firing rate during blue light exposure, but instead

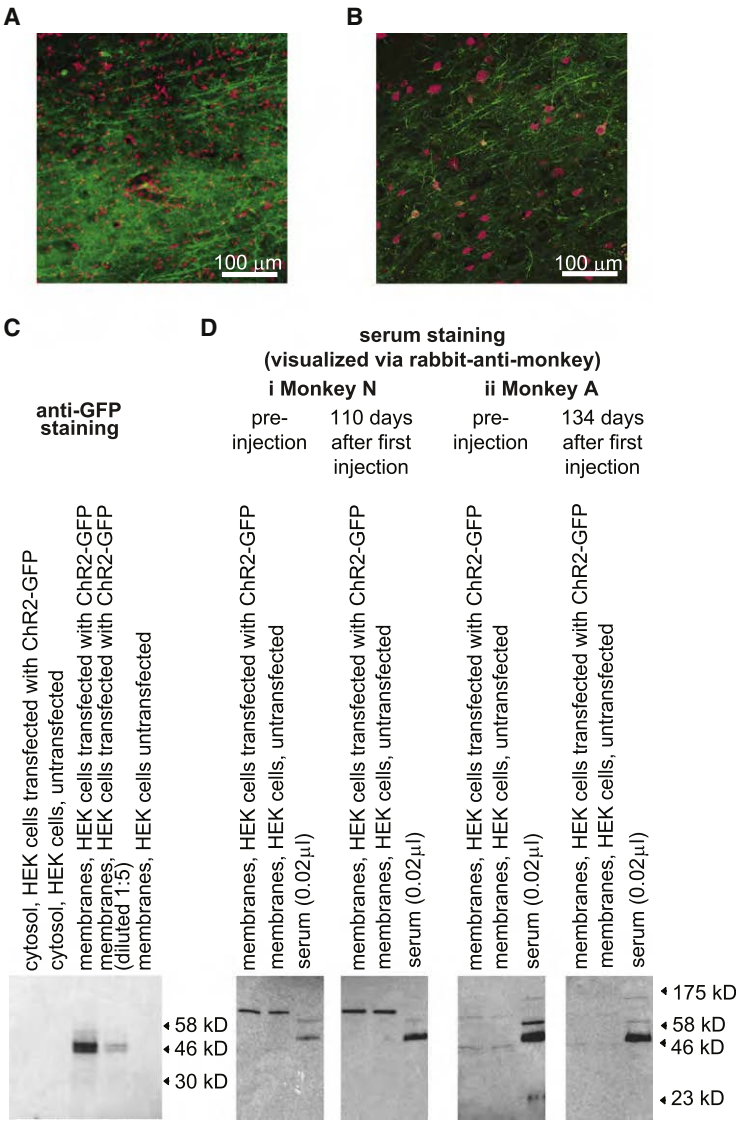

Figure 2. Analyses of Potential Immune Responses against ChR2-GFP-Expressing Neurons in Primate Cortex

(A) Nuclear DNA staining (red; To-Pro-3 stain) of slices of monkey cortex containing ChR2-GFP-expressing neurons (green). (B) Neuronal staining (red; NeuN antibody) of slices of monkey cortex containing ChR2-GFP-expressing neurons (green). (C) Validation of ChR2-GFP expression in HEK cells via western blotting, using anti-GFP antibody. From left to right, lanes show, immunostained with anti-GFP: cytosolic fraction of HEK cells transfected with ChR2-GFP plasmid, cytosolic fraction of untransfected HEK cells, membrane fraction of HEK cells transfected with ChR2-GFP plasmid, membrane fraction (diluted 1:5) of HEK cells transfected with ChR2-GFP plasmid, and membrane fractions of untransfected HEK cells. (D) Assessment of monkey serum reaction to ChR2-GFP, for monkey N (Di) and monkey A (Dii), via western blotting, comparing preinjection (left) to postinjection (right). Membrane fractions of HEK cells transfected with ChR2-GFP (left lane), membrane fractions of untransfected HEK cells (middle lane), and monkey serum samples (right lane) were incubated with monkey serum (1:50 dilution), followed by rabbit-anti-monkey secondary antibody for visualization.

decreased firing rate during light delivery, even after brief illumination (i.e., a single light pulse). We hypothesized that since suppressed units decreased their firing rates without having undergone prior increases in spiking, the observed suppression was due to neural network activity, i.e., recruitment of inhibitory neurons downstream of the driven excitatory neurons. For both the excited and suppressed units, action potential waveforms elicited during light exposure were not different from waveforms observed in the dark ($p > 0.1$ for each of $n = 15$ excited single units; Kolmogorov-Smirnov test comparing waveform shapes in light versus dark; exemplars in Figures 3F and 3G). In regions where excited or suppressed units were found, few light-nonmodulated units were observed (Figure S5). These excited and suppressed units were also observed in the cortex of mice, when excitatory neurons expressing ChR2-GFP were activated by light (Figure S3). Light did, however, result in a low-frequency electrical artifact on our tungsten electrodes in the brain, presumably due to the photoelectric effect; this artifact was removed from our data by high-pass filtering (see Figure S1). Light (80 mW/mm^2 radiant flux out the tip of the fiber) modulated neurons at distances over 1.2 mm away from the fiber (Figure S2).

In the monkey cortex, we recorded 50 excited and 20 suppressed units during illumination with 200 ms blue light pulses. Out of these 70 units, 31 were single units (15 excited, 16 suppressed) and 39 were multiunits (35 excited, 4 suppressed). We pooled multiunits and single units for analysis unless otherwise indicated. Excited and suppressed units had similar baseline firing rates ($p > 0.2$, t test; only single units compared) and similar waveform shapes (see Supplemental Experimental Procedures). For excited units, firing rates increased rapidly at light onset, and then settled to a lower steady-state firing level (Figure 3H). For suppressed units, firing rates fell sharply after a short delay, and remained low for the duration of the light pulse (Figure 3J). For both excited and suppressed units, after light cessation the firing rates often dipped below baseline levels for ~100 ms. We quantified the magnitude of these changes in firing rate during three distinct periods: the first 20 ms of light exposure ("beginning of light"), the period between 20 ms after light onset and 20 ms after light cessation ("steady state"), and during the 20 ms period starting 20 ms after light cessation ("after light"). Excited units fired at 750%, 370%, and 46% of baseline firing rate during these three periods, respectively, in each case significantly different from baseline ($p < 0.0001$ for each, paired t test; Figure 3I). For single units, which yield absolute values of firing rate, excited neurons fired at 37 ± 7 Hz, 16 ± 4 Hz, and 1.3 ± 1 Hz during these three periods (mean ± standard error [SE]; $n = 15$ single units); baseline their firing rates was 6.5 ± 1.3 Hz. In contrast to the excited units, suppressed units did not change their firing rates relative to baseline during the beginning of light period ($p > 0.5$, paired t test; Figure 3K), but reduced their firing rates by 76% and 75%, respectively, during the steady state and after light periods

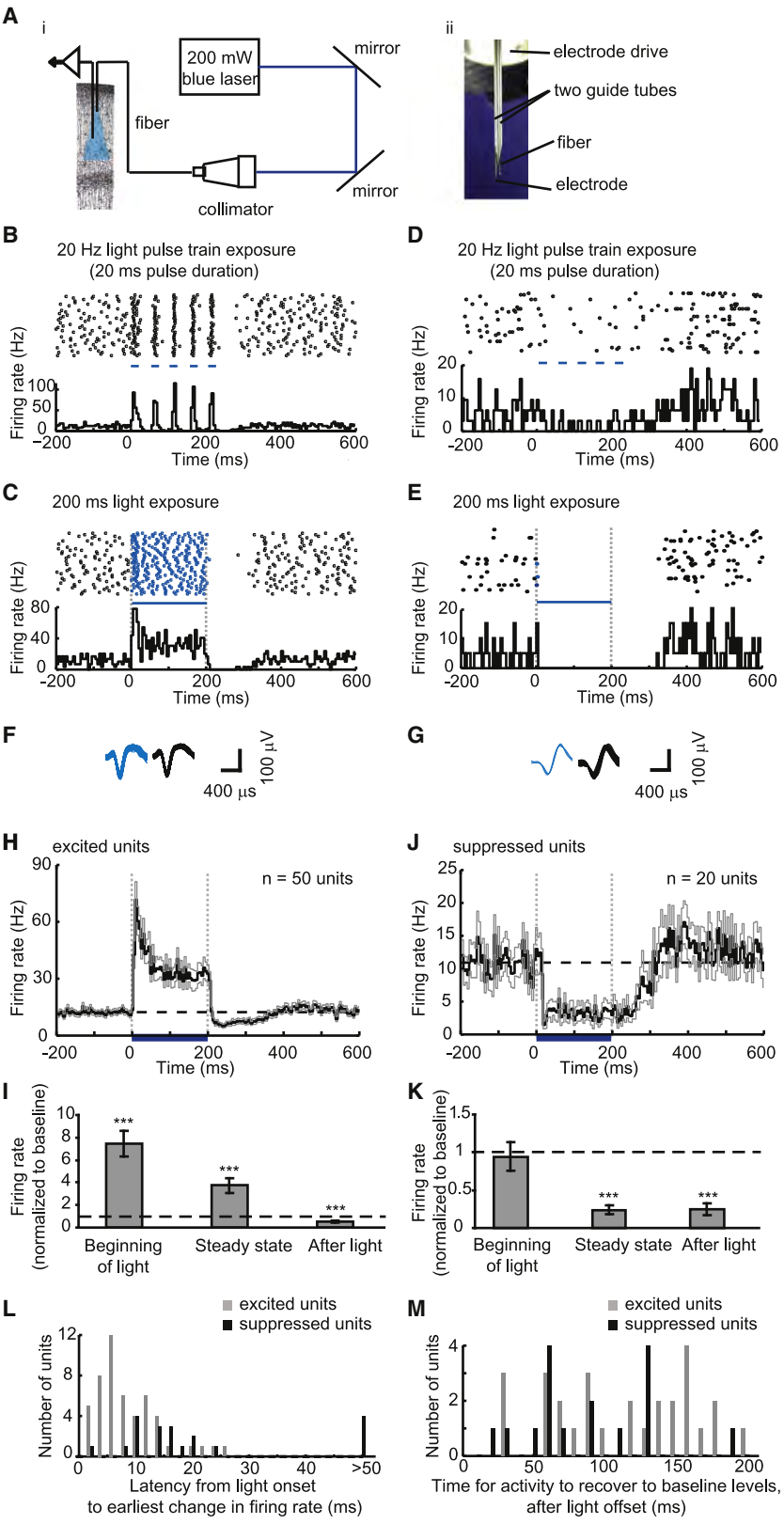

Figure 3. Increases and Decreases in Neural Activity Resulting from Optical Stimulation of Excitatory Neurons

(A) Apparatus for optical activation and electrical recording. (Ai) Schematic. (Aii) Photograph, showing optical fiber (200 μm diameter) and electrode (200 μm shank diameter) in guide tubes. (B and C) Increases in spiking activity in one neuron during blue light illumination (five pulses, 20 ms duration each [B], and 1 pulse, 200 ms duration [C]). In each panel, shown at top is a spike raster plot displaying each spike as a black dot; 40 trials are shown in horizontal rows (in this and subsequent raster plots); shown at bottom is a histogram of instantaneous firing rate, averaged across all trials; bin size, 5 ms (in this and subsequent histogram plots). Periods of blue light illumination are indicated by horizontal blue dashes, in this and subsequent panels. (D and E) Decreases in spiking activity in one neuron during blue light illumination (five pulses, 20 ms duration (D), and one pulse, 200 ms duration [E]). As with (B) and (C), shown at top are spike raster plots and shown at bottom are histograms of instantaneous firing rate. (F and G) Action potential waveforms elicited during light (shown in blue, left) or occurring spontaneously in darkness (shown in black, right), for the neurons plotted in (C) and (E), respectively. (H) Instantaneous firing rate, averaged across all excited units recorded upon 200 ms blue light exposure (black line, mean; gray lines, mean ± SE; n = 50 units). (I) Relative firing rate (i.e., firing rate during the indicated period, divided by baseline firing rate) during the first 20 ms after light onset ("beginning of light"), during the period between 20 ms after light onset and 20 ms after light cessation ("steady state"), and during the 20 ms period starting 20 ms after light cessation ("after light"), for the n = 50 units shown in (H). (***), significantly different ($p < 0.0001$; paired t test) from baseline rate (shown as dotted line); plotted is mean ± SE. (J) Instantaneous firing rate averaged across all suppressed units upon 200 ms blue light exposure (black line, mean; gray lines, mean ± SE; n = 20 units). (K) Relative firing rate, during the beginning of light, steady state, and after light periods, for the n = 20 units shown in (J). (L) Histogram of latencies between light onset and the earliest change in firing rate, for excited units (gray bars, n = 50 units) and suppressed units (black bars, n = 20 units); latencies longer than 50 ms were plotted in a bin labeled ">50." (M) Histogram of time elapsed until activity recovery to baseline after light cessation, for excited (gray bars, n = 28 units) and suppressed (black bars, n = 16 units) units that had lower-than-baseline firing rates during the after light period.

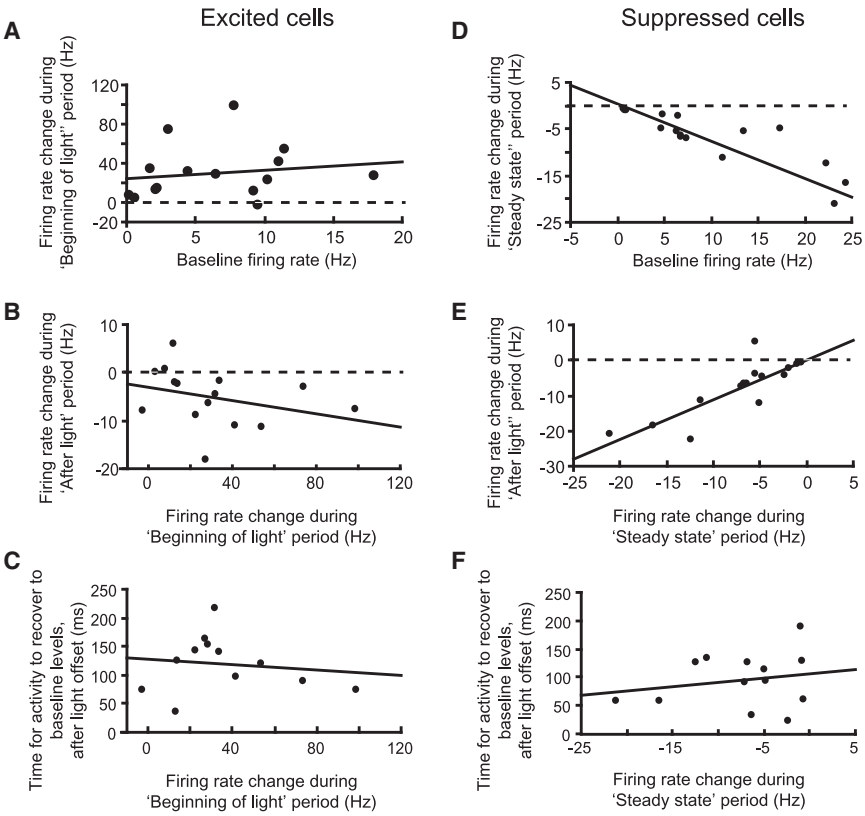

Figure 4. Comparison of Neural Activity Levels within Excited and Suppressed Single Units, before, during, and after Light Exposure

(A) Firing rate change during the beginning of light period (i.e., firing rate during beginning of light minus baseline firing rate) versus baseline firing rate, for excited cells (n = 15 excited single units). (B) Firing rate change during the after light period versus during the beginning of light period, for excited single units. (C) Time elapsed until activity recovery to baseline level after light cessation, versus firing rate change during the beginning of light period, for excited single units. (D) Firing rate change during the steady state period, versus baseline firing rate, for suppressed cells (n = 16 suppressed single units). (E) Firing rate change during the after light period versus during the steady state period, for suppressed single units. (F) Time elapsed until activity recovery to baseline level after light cessation, versus firing rate change during the steady state period, for suppressed single units.

(significantly lower than that during baseline [$p < 0.0001$, paired t test], but not different from each other; $p > 0.8$). Suppressed single units fired at 7.4 ± 1.7 Hz, 3.1 ± 1.0 Hz, and 2.5 ± 1.2 Hz during these three periods, respectively (mean ± SE; n = 16 single units); baseline firing rate was 9.9 ± 2.0 Hz.

We compared the latencies to changes in firing rate between excited versus suppressed units, and found two different, but overlapping, distributions. Excited units rapidly responded to light with latencies of 8.8 ± 0.8 ms (mean ± SE; Figure 3L). This short latency was not different from the first-spike latency of ChR2-positive cultured pyramidal neurons responding to pulses of blue light ($p > 0.6$, unpaired t test; compared to published data in Boyden et al., 2005), consistent with the idea, but not proving, that excited units were ChR2-positive pyramidal cells. In contrast to the short latencies of excited units, suppressed units began decreasing their firing rates 30.8 ± 8.0 ms after light onset (mean ± SE), a latency significantly longer than the latency for the increases in firing rates of excited units ($p < 0.0001$, unpaired t test). This difference is consistent with our hypothesis that suppressed units decreased their firing rates through neural network mechanisms involving inhibitory neuron recruitment, whereas excited units were directly activated by light. After light cessation (after light period), the majority of excited and suppressed units exhibited firing rates below baseline levels (28 out of 50 excited units; 16 out of 20 suppressed units). The time for this reduced firing rate to recover to baseline was similar for excited and suppressed units (Figure 3M, $p > 0.1$, unpaired t test), consistent with the idea that suppressive influences downstream of excitatory neuron activation are mediated by a neural-network-scale phenomenon such as inhibitory neuron recruitment.

To probe the nature of neural suppression further, we examined the activity of single units before, during, and after light exposure. For excited cells, we found that increases in firing rate during optical stimulation were independent of baseline firing rate ($R^2 = 0.025$, $p > 0.5$; Figure 4A; n = 15 excited single units). In addition, decreases in firing rate after light cessation were independent of the light-induced increases in firing rate ($R^2 = 0.096$, $p > 0.2$; Figure 4B). Finally, the time for firing rate to recover to baseline levels after light cessation was independent of prior increases in firing rate ($R^2 = 0.016$, $p > 0.7$; Figure 4C; n = 12 excited single units that decreased activity during the after light period). Thus, excited cells fired before, during, and after light exposure, in independent fashions. In contrast to excited units, for suppressed units decreases in firing rate during light exposure were highly correlated with baseline firing rate ($R^2 = 0.749$, $p < 0.0001$; Figure 4D; n = 16 suppressed single units): for each additional Hz of baseline firing rate, light exposure decreased firing by an additional ~0.6 Hz. In addition, the decrease in firing rate of suppressed neurons after light cessation was correlated with the decrease in firing rate during light exposure ($R^2 = 0.673$, $p < 0.0001$; Figure 4E). However, as for excited cells, the time for the firing rate to recover to baseline level was independent of prior reductions in activity levels for suppressed cells (e.g., during the steady state period; $R^2 = 0.045$, $p > 0.4$; Figure 4F; n = 13 suppressed single units that had significant decreases in activity during the after light period). Thus, for suppressed cells, but not for excited cells, light-induced changes in activity were correlated with baseline activity, as though the magnitudes of spontaneous and light-suppressed activity were both functions of a common neural network state. We further probed the response of excited cells with trains of light pulses at 10, 20,

and 50 Hz (Figure S6), finding that while spike probability fell during long, high-frequency trains, spike timing remained reliable, and therefore ChR2 may subserve the ability to use light to control cortical synchrony.

DISCUSSION

We have demonstrated millisecond-timescale optical activation of excitatory neurons in the frontal cortex of nonhuman primates, using lentivirally delivered ChR2, and have characterized the impact of such optical control on cortical circuits. This work demonstrates the feasibility of applying optogenetic methods to primate neural circuits, and points the way toward the potential use of optical control in a new generation of therapies for the improvement of human health. Immediately, this technology makes it possible to activate a region containing a set of excitatory neurons while avoiding the modulation of fibers of passage, or of neurons projecting into the region. Light stimulation did result in a slow electrical artifact on the metal electrode, which was easily filtered out from our spike recordings. Single viral injections labeled on the order of 1 mm^3 of brain tissue, comparable to the volume illuminated by single optical fibers, suggesting that arrays of viral injectors and optical fibers may enhance the ability to systematically modulate cell and circuit activities during behavior.

We found that whereas many neurons were excited during light activation of excitatory neurons, others were profoundly suppressed during light exposure. In addition, many excited and suppressed cells exhibited a period of reduced neural activity after cessation of light activation. These excited and suppressed effects were also observed in mouse cortical neurons under similar optical stimulation conditions. These effects may be due to biophysical properties of the neurons recorded, for example hyperpolarization after depolarization-induced opening of BK and SK potassium channels (Bekkers, 2000; Sah and Davies, 2000; Storm, 1987; Vogalis et al., 2003). But several independent lines of reasoning support the hypothesis that suppression emerges from recruitment of networks of inhibitory cells downstream of activated ChR2-positive excitatory cells. First, suppressed neurons underwent reductions in spike firing without having undergone prior increases in spike firing, which implies that cell-autonomous mechanisms such as postdepolarization hyperpolarization cannot be the sole mechanism mediating the observed suppression. Second, the latency to the decrease in firing after light onset was significantly longer for suppressed cells than the latency to the increase in firing was for excited cells, consistent with suppressed cells being downstream of light-activated cells. Third, suppressed neurons decreased activity during light exposure in proportion to their basal firing rate, whereas light-driven excitation was independent of basal firing rate, consistent with suppression being mediated through a mechanism related to the one that sustains baseline firing, i.e., network activity. Finally, postillumination reductions in neural activity were similar in duration across excited and suppressed neurons, again suggesting that these effects may be more due to emergent properties of the neural network that a given neuron is embedded in, rather than that cell's autonomous history of activity. Future studies will explore which inhibitory neurons are recruited by excitatory neurons to create activity patterns like those found here; one possibility is that somatostatin-positive interneurons that can be activated by stimulation of single excitatory neurons (Kapfer et al., 2007) could potentially mediate excitation-induced suppression. It will also be interesting to see if such dynamics can subserve oscillatory activity: in Figures 3H and 3J, the rebound depolarization after the end of activity suppression is suggestive of a possible natural timescale of activity fluctuation in the delta-theta range.

Electrical microstimulation is an important tool for both basic neuroscience and for therapeutic neuromodulation, but how it impacts neural circuit dynamics remains unclear. In microstimulation experiments where recording was also performed, some neurons dramatically decreased activity in response to electrical microstimulation (e.g., Butovas et al., 2006; Butovas and Schwarz, 2003; Seidemann et al., 2002). These electrical stimulation-induced decreases possessed some of the same attributes of the suppressions here observed; for example, the duration of the inhibition was largely independent of the amount of activation induced (Butovas and Schwarz, 2003). This inhibition was pharmacologically associated with GABAergic neuron recruitment (Butovas et al., 2006), but it remained unknown whether electrical microstimulation must directly recruit GABAergic neurons, or whether activation of excitatory neurons would be sufficient to create such inhibition. Here we prove that driving excitatory neurons alone is sufficient to result in periods of activity suppression in a significant population of cortical neurons. We found similar responses in mouse neocortex, which suggests that such neural dynamics might be a general property of neocortical circuits under neuromodulation. Thus, even when just one cell type is manipulated, its impact on the brain must be evaluated in the context of the neural network in which it is embedded. Principles must be derived for how to control a circuit, even given a delimited set of cell types to be controlled, in order to achieve a desired physiological, behavioral, or clinical outcome.

Optically activating excitatory neurons is just one step along the path of implementing cell-type-specific optical control in primates. Future viral, promoter, injection, and illumination innovations will need to be developed to match the manipulations possible in mice and other classical genetic model systems. Optical neural silencing strategies for primates will also be critical, perhaps involving light-activated chloride pumps such as halorhodopsins (Halo/NpHR) (Han and Boyden, 2007; Zhang et al., 2007). Especially for questions involving higher-order activity patterns such as neural synchrony, the ability to use ChR2 and Halo in concert to create "informational lesions," in which precise neural patterns are disrupted, may prove especially useful (Han and Boyden, 2007).

Launching the verification of the safety and efficacy of ChR2 function in rhesus macaques is a critical step toward any potential clinical translational path for cell-type-specific optical neural control prosthetics. Given that in many disorders, the functions of specific cell types are compromised, it is possible that the ability to optically remedy aberrant activity in specific cell types will spur precise, side-effect-free treatments for neural disorders. As a first step toward this synthetic neurobiology goal, here we have shown that ChR2 performs efficaciously and without immune attack in the macaque brain, and appears to

be safe over many months despite repeated viral injections and repeated illumination sessions.

EXPERIMENTAL PROCEDURES

Detailed descriptions are provided in the Supplemental Data. All procedures were in accordance with the NIH Guide for Laboratory Animals and approved by the MIT Animal Care and Use and Biosafety Committees. Two rhesus monkeys, 7–11 years of age, weighing 8–15 kg, were equipped for awake headfixed physiology. High-titer replication-incompetent lentivirus encoding for ChR2-GFP was produced and injected into premotor cortex/frontal eye fields, via custom hardware. Optical stimulation proceeded via a 200 μm diameter optical fiber coupled to a 200 mW blue laser. Electrophysiological recording was performed using tungsten electrodes guided parallel to the optical fiber, using independent microdrives. Signal conditioning and acquisition were performed with a Plexon data acquisition system and analyzed with Matlab. The brain of one of the two monkeys was fixed and examined with immunostaining and confocal microscopy.

SUPPLEMENTAL DATA

The supplemental data for this article include Results, Experimental Procedures, and six Figures and can be found at http://www.neuron.org/supplemental/S0896-6273(09)00210-4.

ACKNOWLEDGMENTS

We thank the MIT Division of Comparative Medicine for help with serum collection, and H. Hall and P. Harlen for help with preparing cortical slices. We thank members of the Boyden and Desimone labs, and E. Tehovnik, for their suggestions on the manuscript. This work was supported by NIH-EY002621-31; a HHWF fellowship to X.H.; a McGovern Institute Neurotechnology Award to E.S.B., R.D., and X.H.; grant NIH-EY12848 to A.G.; and grants NIH-EY017292 and EY017921 to R.D. E.S.B. acknowledges support from the NIH Director's New Innovator Award (DP2 OD002002-01), NSF, Department of Defense, NARSAD, Alfred P. Sloan Foundation, Jerry Burnett Foundation, SFN Research Award for Innovation in Neuroscience, MIT Media Lab, MIT McGovern Institute, Benesse Foundation, MIT Neurotechnology Fund, and Wallace H. Coulter Foundation.

Accepted: March 9, 2009
Published: April 29, 2009

REFERENCES

Bekkers, J.M. (2000). Distribution of slow AHP channels on hippocampal CA1 pyramidal neurons. J. Neurophysiol. *83*, 1756–1759.

Bernstein, J.G., Han, X., Henninger, M.A., Ko, E.Y., Qian, X., Franzesi, G.T., McConnell, J.P., Stern, P., Desimone, R., and Boyden, E.S. (2008). Prosthetic systems for therapeutic optical activation and silencing of genetically-targeted neurons. Proc Soc Photo Opt Instrum Eng *6854*, 68540H.

Boyden, E.S., Zhang, F., Bamberg, E., Nagel, G., and Deisseroth, K. (2005). Millisecond-timescale, genetically targeted optical control of neural activity. Nat. Neurosci. *8*, 1263–1268.

Butovas, S., and Schwarz, C. (2003). Spatiotemporal effects of microstimulation in rat neocortex: a parametric study using multielectrode recordings. J. Neurophysiol. *90*, 3024–3039.

Butovas, S., Hormuzdi, S.G., Monyer, H., and Schwarz, C. (2006). Effects of electrically coupled inhibitory networks on local neuronal responses to intracortical microstimulation. J. Neurophysiol. *96*, 1227–1236.

Cahoy, J.D., Emery, B., Kaushal, A., Foo, L.C., Zamanian, J.L., Christopherson, K.S., Xing, Y., Lubischer, J.L., Krieg, P.A., Krupenko, S.A., et al. (2008). A transcriptome database for astrocytes, neurons, and oligodendrocytes: a new resource for understanding brain development and function. J. Neurosci. *28*, 264–278.

Chan, A.W., Chong, K.Y., Martinovich, C., Simerly, C., and Schatten, G. (2001). Transgenic monkeys produced by retroviral gene transfer into mature oocytes. Science *291*, 309–312.

Dittgen, T., Nimmerjahn, A., Komai, S., Licznerski, P., Waters, J., Margrie, T.W., Helmchen, F., Denk, W., Brecht, M., and Osten, P. (2004). Lentivirus-based genetic manipulations of cortical neurons and their optical and electrophysiological monitoring in vivo. Proc. Natl. Acad. Sci. USA *101*, 18206–18211.

Han, X., and Boyden, E.S. (2007). Multiple-color optical activation, silencing, and desynchronization of neural activity, with single-spike temporal resolution. PLoS ONE *2*, e299.

Hendry, S.H., Jones, E.G., Emson, P.C., Lawson, D.E., Heizmann, C.W., and Streit, P. (1989). Two classes of cortical GABA neurons defined by differential calcium binding protein immunoreactivities. Exp. Brain Res. *76*, 467–472.

Houser, C.R., Hendry, S.H., Jones, E.G., and Vaughn, J.E. (1983). Morphological diversity of immunocytochemically identified GABA neurons in the monkey sensory-motor cortex. J. Neurocytol. *12*, 617–638.

Ishizuka, T., Kakuda, M., Araki, R., and Yawo, H. (2006). Kinetic evaluation of photosensitivity in genetically engineered neurons expressing green algae light-gated channels. Neurosci. Res. *54*, 85–94.

Jones, E.G., Huntley, G.W., and Benson, D.L. (1994). Alpha calcium/calmodulin-dependent protein kinase II selectively expressed in a subpopulation of excitatory neurons in monkey sensory-motor cortex: comparison with GAD-67 expression. J. Neurosci. *14*, 611–629.

Kapfer, C., Glickfeld, L.L., Atallah, B.V., and Scanziani, M. (2007). Supralinear increase of recurrent inhibition during sparse activity in the somatosensory cortex. Nat. Neurosci. *10*, 743–753.

Kordower, J.H., Emborg, M.E., Bloch, J., Ma, S.Y., Chu, Y., Leventhal, L., McBride, J., Chen, E.Y., Palfi, S., Roitberg, B.Z., et al. (2000). Neurodegeneration prevented by lentiviral vector delivery of GDNF in primate models of Parkinson's disease. Science *290*, 767–773.

Li, X., Gutierrez, D.V., Hanson, M.G., Han, J., Mark, M.D., Chiel, H., Hegemann, P., Landmesser, L.T., and Herlitze, S. (2005). Fast noninvasive activation and inhibition of neural and network activity by vertebrate rhodopsin and green algae channelrhodopsin. Proc. Natl. Acad. Sci. USA *102*, 17816–17821.

Liu, Z., Richmond, B.J., Murray, E.A., Saunders, R.C., Steenrod, S., Stubblefield, B.K., Montague, D.M., and Ginns, E.I. (2004). DNA targeting of rhinal cortex D2 receptor protein reversibly blocks learning of cues that predict reward. Proc. Natl. Acad. Sci. USA *101*, 12336–12341.

Luo, L., Callaway, E.M., and Svoboda, K. (2008). Genetic dissection of neural circuits. Neuron *57*, 634–660.

McLendon, R.E., and Bigner, D.D. (1994). Immunohistochemistry of the glial fibrillary acidic protein: basic and applied considerations. Brain Pathol. *4*, 221–228.

Nagel, G., Szellas, T., Huhn, W., Kateriya, S., Adeishvili, N., Berthold, P., Ollig, D., Hegemann, P., and Bamberg, E. (2003). Channelrhodopsin-2, a directly light-gated cation-selective membrane channel. Proc. Natl. Acad. Sci. USA *100*, 13940–13945.

Sah, P., and Davies, P. (2000). Calcium-activated potassium currents in mammalian neurons. Clin. Exp. Pharmacol. Physiol. *27*, 657–663.

Seidemann, E., Arieli, A., Grinvald, A., and Slovin, H. (2002). Dynamics of depolarization and hyperpolarization in the frontal cortex and saccade goal. Science *295*, 862–865.

Stettler, D.D., Yamahachi, H., Li, W., Denk, W., and Gilbert, C.D. (2006). Axons and synaptic boutons are highly dynamic in adult visual cortex. Neuron *49*, 877–887.

Storm, J.F. (1987). Action potential repolarization and a fast after-hyperpolarization in rat hippocampal pyramidal cells. J. Physiol. *385*, 733–759.

Tan, E.M., Yamaguchi, Y., Horwitz, G.D., Gosgnach, S., Lein, E.S., Goulding, M., Albright, T.D., and Callaway, E.M. (2006). Selective and quickly reversible

inactivation of mammalian neurons in vivo using the Drosophila allatostatin receptor. Neuron *51*, 157–170.

Tighilet, B., Hashikawa, T., and Jones, E.G. (1998). Cell- and lamina-specific expression and activity-dependent regulation of type II calcium/calmodulin-dependent protein kinase isoforms in monkey visual cortex. J. Neurosci. *18*, 2129–2146.

Vogalis, F., Storm, J.F., and Lancaster, B. (2003). SK channels and the varieties of slow after-hyperpolarizations in neurons. Eur. J. Neurosci. *18*, 3155–3166.

Yang, S.H., Cheng, P.H., Banta, H., Piotrowska-Nitsche, K., Yang, J.J., Cheng, E.C., Snyder, B., Larkin, K., Liu, J., Orkin, J., et al. (2008). Towards a transgenic model of Huntington's disease in a non-human primate. Nature *453*, 921–924.

Zhang, F., Wang, L.P., Brauner, M., Liewald, J.F., Kay, K., Watzke, N., Wood, P.G., Bamberg, E., Nagel, G., Gottschalk, A., and Deisseroth, K. (2007). Multimodal fast optical interrogation of neural circuitry. Nature *446*, 633–639.

Neuron, volume *61*

Supplemental Data

Millisecond-Timescale Optical Control of Neural Dynamics in the Nonhuman Primate Brain

Xue Han, Xiaofeng Qian, Jacob G. Bernstein, Hui-hui Zhou, Giovanni Talei Franzesi, Patrick Stern, Roderick T. Bronson, Ann M. Graybiel, Robert Desimone, and Edward S. Boyden

SUPPLEMENTAL RESULTS

Safety assessments. There are no defined immunostimulatory activities known to date to be associated with these light-activated channels. However, the membrane protein ChR2 (and the soluble protein GFP) are exogenously derived from non-primate organisms, raising the possibility that expression of such molecules in specific cells could, in theory, provoke an immune attack on those cells. Thus, we performed a series of different analyses to explore this possibility, focusing on brain regions with high densities of ChR2-GFP positive cells that were not immediately abutting the scar left by the cannula used for viral infusion. First, in the histological analysis of monkey N, performed 110 days after the first viral injection (and 81 days after the last viral injection), we saw ChR2-GFP expression in many excitatory cells (up to ~80%, near the center of injection sites). The widespread persistence of expression of these exogenous proteins in healthy-looking cells, several months after viral gene delivery**,** implies a lack of cytotoxic immune response against cells expressing ChR2-GFP (e.g., compare to (Aktas et al., 2005; Bien et al., 2002; Murphy et al., 2007)). Second, the recordings of neural activity modulated by light (**Figs. 3-4**) indicated functional expression of ChR2 in neurons throughout the period of the experiment (over 8 months for monkey A), even after many sessions of repeated blue-light illumination of the same set of cells. Third, to assess cellular architecture at the site of ChR2-GFP expression, we stained either the nuclei of all cells with the nucleic acid stain To-Pro-3 (**Fig. 2A**), or just the nuclei of neuronal cells with antibody to the neuron-specific nuclear marker NeuN (**Fig. 2B**). We did not detect disruptions of cellular architecture, even in regions with a high density of ChR2-GFP-expressing cells. Fourth, we measured the density of reactive astrocytes, using GFAP staining (Ridet et al., 1997). The density of GFAP-positive cells was identical in regions with a high density of ChR2-GFP expressing cells (13.5 ± 1.5 GFAP-positive cells per $2.5*10^6$ μm^3, mean ± SE) and in regions with no ChR2-GFP expressing cells, far away from the cannula (14.4 ± 1.5 GFAP positive cells per volume) ($p > 0.5$, unpaired t-test; n = 13 fields of view each), confirming that ChR2-GFP expression did not evoke gliosis. This lack of disorganization and immune cell infiltration was consistent with the excellent appearance of the ChR2-GFP-positive neurons (see also **Fig. 1**), as well as the physiological health of the neurons (**Fig. 3-4)**, even after many months of viral expression, and strongly suggests that a functional immune response did not occur.

Finally, we took a step towards assessing the presence of antibodies against ChR2-GFP in the serum of the two monkeys by Western blotting samples of their serum against purified membranes of HEK cells transfected with ChR2-GFP plasmids. Control western blotting with a rabbit polyclonal antibody against whole GFP consistently labeled two bands around 46 kD (approximately 75% of the molecular weight of the entire ChR2-GFP fusion protein, suggesting that we were consistently isolating two sizable fragments of the entire protein). These bands were detected only in the membrane fraction of HEK cells transfected with ChR2-GFP plasmid, and not in the cytosolic fraction of HEK cells transfected with ChR2-GFP plasmid, implying that we are indeed isolating a membrane-localized protein (**Fig. 2C**). These bands were not detected in membranes of untransfected HEK cells, confirming specificity of the antibody staining. Western blotting with monkey serum (1:50), obtained before vs. after viral injections, detected in neither case any specific reactivity to membranes of HEK cells transfected with ChR2-GFP, when compared to membranes of untransfected HEK cells (**Fig. 2D**). In greater detail: for both monkeys, there was nonspecific binding of serum to membranes of HEK cells, but there was no difference in binding of serum to membranes of ChR2-GFP transfected vs. untransfected HEK cells. Furthermore, there was no difference in the binding of serum to a given membrane extract, when we compared before vs. after virus injection. (The observed bands in the blotting of monkey serum against untransfected HEK cells do, however, suggest that our Western blot is capable of detecting some immune response in monkey serum, to a molecule found in untransfected cultured HEK cells.) Finally, we assessed the presence of antibodies in the monkey serum, by running the serum itself in a lane (**Fig. 2D**), and using a secondary antibody against monkey antibodies for visualization; this procedure revealed bands appropriate for antibodies in the serum (given that the heavy chain weighs ~50 kD). Taken together, these lines of evidence support a lack of productive immune response following neuron-specific expression of ChR2-GFP in primate brain.

Optical artifact at low frequencies on metal electrode tips in saline. When electrodes made of tungsten (as used in the in vivo recordings in monkey cortex reported in this paper) were immersed in saline, we observed a voltage deflection that occurred when the electrode tip was illuminated with light. Shown in **Supplemental Fig. 1A** are traces recorded on a tungsten electrode in saline being illuminated by a pulsed laser beam (120 mW). This voltage deflection was qualitatively proportional, in amplitude, to the magnitude of the incident light; the artifact was still visible when incident light power was reduced to 1% of the value that elicited the artifact in **Supplemental Fig. 1A**. The voltage slowly evolved over many tens of milliseconds, and accordingly was only recorded when the electrode voltage was measured on the low-frequency channel of the Plexon amplifier ("field potential channel," 0.7-170 Hz; **Supplemental Fig. 1Ai, ii,** *top traces*). This voltage deflection was not recorded when the electrode voltage was recorded on the high-frequency channel of the Plexon amplifier ("spike channel," 250-8000 Hz; **Supplemental Fig. 1Ai, ii,** *bottom traces*).

When light illuminated parts of the electrode other than the tip, no artifact was recorded; only illumination of the tip-saline interface resulted in the voltage transient. This phenomenon is consistent with a classical photoelectrochemical finding, the Becquerel

effect, in which illumination of an electrode placed in saline can produce a voltage on the electrode (Gratzel, 2001; Honda, 2004). Consistent with the generality of the Becquerel effect as a property of electrode-electrolyte interfaces, we observed this artifact even when the electrode material was switched to an alternative material, such as stainless steel, platinum-iridium, silver/silver chloride, gold, nichrome, or copper (data not shown). For a given positioning of electrode and light beam, and a given light power intensity, artifacts were observed to be stable in amplitude and timecourse, throughout the delivery of repeated light pulses. The artifact has been reported by another group using channelrhodopsin-2 as well, using silver electrodes for recording cortical responses (Ayling et al., 2009).

Similar slowly-evolving voltage deflections were observed when tungsten electrodes were used to record neural activity in the brain within a few millimeters of the fiber tip, during optical stimulation (**Supplemental Fig. 1Bi, ii,** *top traces*) with a radiant flux of 80 mW/mm^2 out the tip of the optical fiber (sufficient to activate neurons within about a cubic millimeter of brain, **Supplemental Figs. 2** and **5**). It is possible that part of this voltage deflection is due to the local field potential (LFP), but it is not possible in these data to resolve the LFP from the artifact. At a distance 1 millimeter away from the optical fiber tip, a distance at which optical neural activation was greatly reduced (**Supplemental Fig. 2**), the amplitude of the voltage deflection was reduced, but nonzero. Because the voltage deflection was slowly-evolving over many tens of milliseconds, spike waveforms were detected without corruption by the artifact, in the high-frequency channel of the Plexon amplifier (**Supplemental Fig. 1Bi, ii,** *bottom traces*). However, local field potentials and field oscillations, which reflect coherent neural dynamics in the range of Hz to tens of Hz, may be difficult to isolate from this Becquerel artifact using the electrodes here tested. We have not seen the artifact with pulled glass micropipettes (such as previously used in Boyden et al., 2005 and Han and Boyden, 2007, or in the mouse recordings described below). Thus, for recordings of local field potentials and other slow signals of importance for neuroscience, hollow glass electrodes may prove useful.

Dependence of light modulation of ChR2-expressing neurons upon light power and fiber position. We investigated the dependence of optical neural excitation on light amplitude by systematically decreasing the light intensity while recording from excited cells. We found, consistent with earlier reports in cultured neurons and in transgenic mice (e.g., (Boyden et al., 2005; Wang et al., 2007)), that light power intensity on the order of several mW/mm^2 were optimal for driving neural activity (n = 11; **Supplemental Fig. 2Ai-iii**). To explore the geometry of this situation for the primate brain, we recorded excited units, holding laser power intensity constant at 80 mW/mm^2, and retracted the optical fiber from its most efficacious position, in 200 micron increments. As expected, light-driven spiking decreased as the fiber was retracted (n = 7; **Supplemental Fig. 2Bi-iii**). Excited units lost their optical modulation fully when the optical fiber was retracted by an average of 1.2 ± 0.4 mm (mean ± SD), suggesting that a volume of about a cubic millimeter could be addressed in primate cortex, by a single fiber, at this power level. Interestingly, there was a noticeable trend for the after-light suppression of activity to vanish at lower light power intensities than did the beginning-of-light excitation of activity (e.g., compare the curves in **Supplemental Fig. 2Ai vs. Aiii**, or the curves in

Supplemental Fig. 2Bi vs. Biii). This observation is consistent with the idea that the suppression is mediated by distributed neural networks (presumably part of which is illuminated, even when the neuron being recorded is not being illuminated), whereas excitation requires immediate light delivery to the neuron being recorded (or perhaps to neurons very close by).

Excited and suppressed neural responses in mouse frontal cortex. To test whether the excited vs. suppressed responses observed (**Fig. 3**) were primate-specific, we repeated the experiment in rodent cortex. We injected FCK-ChR2-GFP lentivirus into the mouse frontal cortex (0.62 mm anterior, 0.5 mm lateral, and 0.5 mm deep, relative to bregma), so that ChR2-GFP was selectively expressed in excitatory neurons (37 of 37 GFP-positive neurons counted were α-CaMKII positive, whereas 0 of 32 GFP-positive neurons counted were GABA-positive). 4 weeks to 8 months after virus injection, we performed extracellular recordings on awake, head-fixed mice. 200 ms-duration blue light pulse illumination of ChR2-GFP-expressing excitatory neurons evoked both excited and suppressed responses in frontal cortical neurons (**Supplemental Fig. 3**). Thus, the heterogeneous responses observed in different neurons in the frontal cortex are not unique to the primate, but are also present in rodents, suggesting that simultaneous excited and suppressed responses may be a general property of cortical neural networks upon excitatory cell activation.

Spatial properties of viral labeling in primate frontal cortex. To assess the spatial extent of cells labeled by a single 1 μL virus injection in primate frontal cortex, we identified 6 well-isolated injection sites with clear borders and clear central cannula scars (such as the one shown in **Fig. 1D**). To estimate the diameter of the sphere containing ChR2-GFP expressing cells, we measured the fluorescence magnitudes along lines through the centers of virus injection sites (avoiding the cannula scar), as assessed in coronal slices (**Supplemental Fig. 4)**. Each injection of ~ 1 μl virus labeled a spherical region of ~1.4 mm in diameter (1.4 ± 0.5 mm, mean ± standard deviation (SD); n = 6 spheres of cells); the center cannula scar had an average diameter of 0.29 ± 0.07 mm (mean ± standard deviation; n = 6), similar to the actual diameter of the cannulas here used, of 0.25 mm.

Distribution of response types along individual electrode tracks. To probe the spatial distribution of excited and suppressed units, as well as of non-responsive units, we recorded neural responses in an unbiased fashion by advancing the electrode in 300 μm steps along a track, while keeping the fiber immobilized. The electrode position was, at each location, adjusted ($\pm$ 40 microns) in the dark to optimize neural recording quality, and then illumination was performed to assess whether the recorded units fell into one of three response categories: excited, suppressed, or no response. Above or below certain depths along the track, presumably defined by the virus injection ball diameter (see above), chiefly unresponsive units were found. Between the farthest-separated depths along a track where units responded to light (e.g., either with excitation or suppression), practically all units recorded between these two depths were either excited or suppressed during light exposure (**Supplemental Fig. 5**), with only one non-responsive unit found in between responsive units during the five experiments shown. The distance between the

highest and lowest units recorded that were modulated by light ranged from 0.9-1.5 mm, consistent with the measurements of viral labeling (**Supplemental Fig. 4**) and the measurements of light delivery volume (**Supplemental Fig. 2**). Note that since units may have been multiunits, this experiment puts a lower bound on the fraction of non-responsive neurons in the observed regions (since if multiple neurons are recorded together and classified as one multiunit, then if any of the neurons are light-modulated, the entire multiunit will likely be classified as light-modulated). However, the fact that almost all cells recorded were modulated by light is consistent with the idea that the observed modulations were largely mediated by neural network-propagated activity, as the fraction of cells virally infected was significantly lower than 100%.

Rhythmic network activity mediated by ChR2 drive of excitatory cells in vivo. Rhythmic and oscillatory activity in the brain have been associated with many cognitive, emotional, sensory, and motor functions, raising the possibility that the ability to optically alter brain rhythms could lead to a better understanding of the causal role of such network dynamics in normal and pathological behavior. Accordingly, we probed the temporal precision of ChR2-driven network activity in primate cortex by exposing excited units to extended 10, 20, and 50 Hz trains of blue light pulses (pulse durations 20, 20, and 10 ms respectively) (**Supplemental Fig. 6**). Spike rates (measured during the 20 ms after the onset of each light pulse) elicited by each pulse declined somewhat during the course of each train, as evidenced by lower steady-state firing rates (mean response to the last 5 light pulses) than maximum firing rates (resulting from the first light pulse of the train) (10 Hz: $p < 0.005$, paired t-test, $n = 8$ units; 20 Hz: $p < 0.005$, $n = 14$ units; 50 Hz: $p < 0.05$, $n = 9$ units). In the steady state, light pulses resulted in spike rates that were 70%, 48% and 55% of those elicited by the first light pulses for 10 Hz, 20 Hz and 50 Hz trains, respectively (**Supplemental Fig. 6Aii, Bii, Cii**). Thus, while spiking could still be reliably elicited by pulse train protocols over an extended time, the probability of firing decreased somewhat throughout such trains, especially at pulse rates 20 Hz and higher. Even so, the trial-to-trial jitter of the spikes was ~4 ms, averaged across units (**Supplemental Fig. 6Aiii, Biii, Ciii)**, and did not change throughout the trains ($p > 0.1$ for all frequencies, paired t-test). Thus, spike timing remained reliable across a wide range of frequencies, despite a reduction in firing probability throughout long, high-frequency pulse trains, suggesting that ChR2-mediated drive of excitatory cells may enable the probing of the role of neural synchrony in cortical computation.

SUPPLEMENTAL FIGURE LEGENDS

Supplemental Figure 1. Voltage deflections observed on tungsten electrodes immersed in saline (**A**) or brain (**B**), upon tip exposure to 200 ms blue light pulses (**i**) or trains of 10 ms blue light pulses delivered at 50 Hz (**ii**). Light pulses are indicated by blue dashes. Electrode data was hardware filtered using two data acquisition channels operating in parallel, yielding a low-frequency component ("field potential channel") and a high-frequency component ("spike channel"). For the "spike channel" traces taken in brain (**B**), spikes were grouped into 100 ms bins, and then the binned spikes were displayed beneath corresponding parts of the simultaneously acquired "field potential channel"

signal (59 and 53 repeated light exposures for **Bi** and **Bii** respectively). (Shown are the spikes in 8 such bins – the 2 bins before light onset, the 2 bins during the light delivery period, and the 4 bins after light cessation.) For all other signals shown, 10 overlaid traces are plotted.

Supplemental Figure 2. Light intensity dependence of neural activity driven by ChR2-mediated activation of excitatory neurons. **A**, neural activity during 'Beginning of light' (**i**), 'Steady state' (**ii**), and 'After light' (**iii**) time periods, upon illumination with different light power intensities (plotted is mean ± SE; n = 11 excited units). **B**, neural activity during 'Beginning of light' (**i**), 'Steady state' (**ii**), and 'After light' (**iii**) periods, when optical fibers were retracted, holding the electrode still (plotted is mean ± SE; n = 7 excited units).

Supplemental Figure 3. Increases and decreases in firing rates of neurons in mouse frontal cortex, during optical stimulation of excitatory neurons. **A**, increases in spiking activity in one neuron during blue light illumination (200 ms duration). *Top,* spike raster plot displaying each spike as a black dot; 25 trials are shown in horizontal rows, in this and subsequent raster plots; *bottom*, histogram of instantaneous firing rate (averaged across all trials; bin size, 5 ms, in this and subsequent histogram plots). **B**, decreases in spiking activity in one neuron during blue light illumination (200 ms duration). *Top,* spike raster plot; *bottom*, histogram of instantaneous firing rate.

Supplemental Figure 4. Fluorescence magnitudes measured along lines taken through the centers of spheres of virally-labeled neurons, each created by one injection of 1 microliter of ChR2-GFP lentivirus. Shown are the mean (black lines) and the mean $\pm$ SD (gray lines) for n = 6 well-isolated spheres of virally-labeled cells.

Supplemental Figure 5. Quantitation of the number of light-responsive and light-unresponsive units detected along five individual electrode tracks, each sampled every 300 microns. The farthest-separated depths where units responded to light were first identified, and each unit recorded between those two depths was then classified according to its activity profile – excitation, suppression, or nonresponsive – during light illumination.

Supplemental Figure 6. Driving oscillatory cortical activity by activating ChR2 expressing excitatory neurons with rhythmic blue light pulse trains, at 10 Hz (**A**), 20 Hz (**B**), and 50 Hz (**C**). For each of these three pulse rates, plotted in subpanel **i** is the histogram of instantaneous firing rate (bin size, 5 ms) averaged across all excited units tested (black lines, mean; gray lines, mean ± SE; n = 8 units for 10 Hz, n = 14 units for 20 Hz, and n = 9 units for 50 Hz). Plotted in subpanel **ii** is the firing rate divided by baseline firing rate, during the 20 ms following the onset of each light pulse, and averaged across all excited units tested (mean ± SE)). Plotted in subpanel **iii** is the jitter of spike times elicited by each pulse, calculated as the across-trial standard deviation of the time of the first spike elicited within 20 ms of each light pulse onset and averaged across all excited units tested (mean ± SE).

SUPPLEMENTAL EXPERIMENTAL PROCEDURES

Virus design and production. Replication-incompetent VSVg-pseudotyped lentivirus was produced via triple transfection of FCK-ChR2-GFP lentiviral plasmid (available at http://www.addgene.org/pgvec1?f=c&cmd=findpl&identifier=15814), the viral helper plasmid (pΔ8.74, information at http://www.addgene.org/pgvec1?vectorid=5682&f=v&cmd=showvecinfo), and the pseudotyping plasmid pMD2.G, encoding for the VSVg coat protein (http://www.addgene.org/pgvec1?f=c&cmd=findpl&identifier=12259). VSVg was used because it enables viral infection of a wide range of cell types, including neurons *in vivo* (Naldini et al., 1996). HEK293FT cells (Invitrogen) were plated onto four T175 flasks in D10 medium (DMEM + 10% FBS + 1% penicillin-streptomycin + 1% sodium pyruvate). At near 100% confluence, cells were transfected with DNA (per flask: 22 μg FCK-ChR2-GFP, 15 μg pΔ8.74, 7 μg pMD2.G, 132 μL Fugene 6, brought up to 4.5 mL with DMEM, mixed according to the Fugene instructions, and then added to 16 mL of D10). 24 hours later, the cells were given 20 mL of virus production media (Ultraculture (Lonza) + 1% penicillin-streptomycin + 1% sodium pyruvate +1% sodium butyrate). 48 hours later, the supernatant was spun down at 2000 rpm in a Beckman benchtop Allegra centrifuge for 5 min, filtered through a 0.45 micron filter, and then ultracentrifuged at 22000 rpm in a SW-28 rotor, through a 20% sucrose + phosphate buffered saline (PBS) cushion, for 2 hours at 4°C. The pellets were then slowly resuspended in 30-100 microliters of PBS, and aliquotted in single-use aliquots for storage at −80°C. This protocol enabled production of clean, non-toxic, high-titer (roughly estimated at ~10^9 infectious units/mL) lentivirus for injection into the brain.

General surgical procedures. Two rhesus monkeys (*Macaca mulatta*), 7-11 years of age, weighing 8-15 kg, were used. All procedures were in accordance with the National Institutes of Health Guide for the care and use of Laboratory Animals and approved by the Massachusetts Institute of Technology Animal Care and Use Committee. Under isoflurane anesthesia, a titanium headpost and recording chambers were surgically affixed to the skull, and a craniotomy opened up in one or more of the chambers, according to MRI-determined coordinates for the periarcuate regions (premotor/FEF areas) of the frontal cortex.

Virus injection. The virus was injected through a 31-gauge stainless steel cannula held in a microdrive (Plexon NAN Drive) attached to the recording chamber while the monkey was seated in a primate chair. The cannula was connected via polyethylene tubing to a Hamilton syringe, placed in a syringe pump (Harvard Apparatus), and the syringe, tubing, and cannula filled with silicone oil (Sigma). To insure the ability to both target virus to the desired area, and to return to the same site later for reliable electrophysiology and optical control, we designed a custom 3-D targeting grid using Solidworks (Solidworks Corp.), and printed it out of acrylic (VisiJet SR 200 Plastic Material acrylic) with a 3-D printer with ~50-micron resolution (3D Systems, Inc.). This grid is analogous to commercially available grids from Crist Instrument Co., but tuned for the specific geometries of interest for this joint electrical-optical experiment. One microliter of virus

was injected over a 10 minute period. We then waited an extra 10 minutes for the virus to diffuse away from the site of injection before withdrawing the cannula at a slow rate of 0.12-0.3 mm/min.

The injection strategy was designed to target cortical tissue on each side (posterior and anterior) of the arcuate sulcus (i.e., premotor cortex and FEF, respectively). Thus, to hit the deepest targets of the sulcus, a deeper termination point was required (i.e., we stopped the injector 7 mm below the dura) than to hit targets more anterior or more posterior to the sulcus (i.e., we stopped the injector 5 mm below the dura). The angle of the injection was approximately vertical, and ultimately governed by the placement of the chamber on the skull. Viral injection was accomplished by lowering a 31-gauge steel cannula (250 microns in diameter) into a given site in the grid, targeting the depth as described above, and then injecting 1 μL of FCK-ChR2-GFP virus at that depth. Then, we repeatedly (4-6 times, as appropriate) retracted the injector in 1 mm steps, injecting an additional 1 μL each time, until the cannula was fully retracted. In this way, we attempted to label large regions on both sides of the arcuate sulcus.

Optical stimulation hardware. A 200 mW blue laser (A-L473-200, Aixiz) was coupled to a 200 micron-diameter optical fiber (FIBER-200-UV, Ocean Optics, although sometimes we also used 100 micron fibers) through a homebuilt collimator setup (AC254-040-A1-ML lens, mounted on a modified SM1L20 lens tube, and attached to a SM1SMA fiber adapter, the assembly of which was mounted on a KM100T mirror mount, all from Thorlabs). To prepare the fiber to connect to our homebuilt collimator assembly, we used an SMA connector terminator kit (TERM-KIT, Ocean Optics). The laser, collimator, and mirrors (BB1-E02, mounted on KM100 mirror mounts, Thorlabs), were mounted on a standard optics breadboard (MB1824, Thorlabs), as outlined in (Bernstein et al., 2008). Laser light power was measured with an 818-SL photodetector (Newport Co.)

The fiber was then placed into a stainless steel cannula slightly larger than the optical fiber, and then guided into the brain, using the same electrode drive described above. The laser was controlled via TTL pulses driven by a pulse generator (DS8000, WPI Inc.), with the timing controlled by a computer through the software package, Cortex (http://www.cortex.salk.edu/).

Electrophysiological recording and optical stimulation. Standard tungsten electrodes of 1-2 MΩ resistance (FHC, Inc.) were guided into the brain along a track parallel to the fiber (separated by 0-600 μm), via a second drive. The guide tubes holding the electrode and holding the fiber were often glued parallel to one another, so that fibers and electrodes would remain laterally spaced within 0.6 mm of one another throughout the experiment (recording more lateral to the fiber reduced the probability of obtaining optically modulated cells, although we did not quantitate this in detail). Fibers and electrodes were lowered separately through their respective guide tubes at a slow rate of ~1.5 μm/s to minimize any potential deformation of the cortical surface. Guide tubes did not enter the brain, but instead rested outside the dura; only the fibers and electrodes entered, lowered through the guide tubes.

Data amplification, filtering and acquisition were performed with a Multichannel Acquisition Processor (MAP) system (Plexon, Inc.), which contains multiple data acquisition channels. Each data acquisition channel is split into two parallel channels and filtered with two different bandpass filters to reveal content at different frequencies. The "spike channel" used throughout this paper is defined by Plexon as 250 Hz – 8 kHz and sampled at 40 kHz. The other channel, the "field potential channel," is defined by Plexon as 0.7 Hz -170 Hz. Spikes recorded on the spike channel were semi-automatically detected using an interactively-set threshold, and the spike waveforms were offline sorted to distinguish putative single vs. putative multiple units using principal component analysis (PCA) (Offline Sorter, Plexon, Inc.). Most of the neurons recorded had broad spike waveforms with trough-to-peak duration >250 μs (3 out of 31 single neurons had trough-to-peak waveform durations of 100-200 μs, and the rest had trough-to-peak waveform durations of 250-425 μs), indicating that most of the recorded neurons were putative excitatory neurons (Mitchell et al., 2007). Spike timing was defined as the moment of threshold crossing. Light resulted in a slow artifact on the electrode (**Supplemental Fig. 1**), which was easily separable from the spike trains through high-pass filtering.

During the experiment, one fiber and one or more electrodes were lowered into the brain of an awake headfixed monkey, and optical stimulation was performed while units were recorded. During the recording period, the monkeys were awake and freely viewing, in a dimly lit room. Our targets in arcuate sulcus contain premotor areas; we did not observe overt eye or limb movements during experiments with the stimuli used. Occasional juice rewards were delivered to insure alertness, but no tasks nor reward contingencies were scheduled in the described recording sessions. Our recording strategy was to position the electrode near the fiber by searching for the slow light-induced artifact, and then optimizing the electrode position to record neurons. Subregions of the targeted areas could be found in which no units were modulated by light, and subregions were also found in which almost 100% of the units were modulated by light (**Supplemental Fig. 5**).

Artifact characterization in saline. Electrodes were positioned in saline and targeted by the laser beam. Voltage deflections were amplified, filtered and acquired with a Multichannel Acquisition Processor (MAP) system (Plexon, Inc.). Specifically, the "field potential channel" is defined by Plexon as 0.7-170 Hz and sampled at 1 kHz or 20 kHz. The "spike channel" is defined by Plexon as 250 Hz – 8 kHz and sampled at 20 kHz or 40 kHz.

Electrophysiology data analysis. Electrophysiological data analysis was performed using MATLAB (Mathworks, Inc.). Light-modulated neurons were identified and classified by performing a paired t-test, for each neuron, between the firing rate during the 200 ms period before light onset ('baseline firing rate') vs. during the period of light exposure, across all trials for that neuron, and thresholded at the $p < 0.05$ significance level. Units that showed significant increases in firing rate during any of three time periods – the first 20 ms of light exposure ('Beginning of light'), the period between 20 ms after light onset and 20ms after light cessation ('Steady state'), and during the 20 ms

period starting 20 ms after light cessation ('After light') – were defined as excited units. Units that showed no increase in firing rate during any of these three periods, but showed reduction in firing rate during any of the periods, were defined as suppressed units. To determine the latency between light onset and the neural response (or, for **Fig. 3M**, the time for after-light suppression to recover back to baseline), we swept a 6 ms-long sliding window through the electrophysiology data and looked for the earliest 6 ms period that deviated from baseline firing rate, as assessed by performing a paired t-test for the firing rate during each window vs. during the baseline period, across all trials for each neuron. Latency was defined as the time from light onset to the time at which firing rate was significantly different from baseline for the following 12 ms. Normalizing firing rate at a given timepoint to baseline was performed by taking the ratio of firing rate at that timepoint, to the baseline firing rate. Firing rate change during a given period was defined as the firing rate during that period, minus the baseline firing rate. Jitter was defined as the standard deviation, across repeated trials, of the timing of the first spike that occurred after the onset of a light pulse.

Mouse optical activation and recording. Adult Swiss Webster or C57 mice were used. All procedures were in accordance with the National Institutes of Health Guide for the care and use of Laboratory Animals and approved by the Massachusetts Institute of Technology Animal Care and Use Committee. Under isoflurane anesthesia, 1 μL lentivirus made with FCK-ChR2-GFP was injected through a craniotomy to the premotor area (0.62 mm anterior, 0.5 mm lateral, and 0.5 mm deep, relative to bregma). A custom-fabricated plastic headpost was affixed to the skull, and the craniotomy was protected with agar and covered with a plastic plate. Recordings (cell-attached or extracellular recordings) were made on headfixed, awake mice up to 8 months after virus injection, using glass microelectrodes of ~5MΩ filled with PBS, containing silver/silver-chloride wire electrodes. Signals were amplified with a Multiclamp 700B amplifier, digitized with a Digidata 1440 and acquired with pClamp 10 (Molecular Devices). Data analysis was with Matlab.

Histology and immunofluorescence. One of the two monkeys, Monkey N, weight 8.6 kg, was deeply anesthetized with an overdose of pentobarbital (>70 mg/kg, i.v.), and then the borders of the 3-D targeting grid were marked in the brain by insertion of 18-gauge cannulas into grid holes near the corners. Then the animal was immediately perfused through the left ventricle, first with phosphate buffered saline (PBS; pH 7.3) (2 liters), then with 4% paraformaldehyde in PBS (4 liters), followed by 2 liters of PBS. The cannulas were then removed, and the brain was blocked and cryoprotected in PBS with 20% glycerol + 0.1% sodium azide (>2 days). Brains were then cut into 60 μm coronal sections on a sliding microtome, and stored in PBS + 0.1% sodium azide.

Brain slices were washed and permeabilized 3 times for 30 minutes each in a solution containing PBS, 100 mM glycine, and 0.5% triton X-100 (PTG solution), and then blocked for 2 hours in PTG + 2% normal goat serum from Jackson Immunochemicals (PTB solution). Slices were then incubated with primary antibody in PTB solution overnight at 4^{o}C on a shaker, then washed 4 times for 30 minutes each with PTG solution, and then incubated in the secondary antibody in PTB solution for 2 hours at

room temperature. Finally, the slices were washed 3 times for 30 minutes each with PTG solution, and for 30 minutes in PBS + 100 mM glycine. Antibodies and stains used were rabbit anti-α-CaMKII (1:50, Santa Cruz Biotechnology), rabbit anti-GABA (1:500, Sigma), rabbit anti-GFAP (1:1000, Upstate), mouse anti-NeuN (1:1000, Chemicon), To-Pro–3 iodide (1:2000, Invitrogen), chicken anti-GFP (1:500, Chemicon), Alexa 488 goat anti-chicken (1:500), and Alexa 568 goat anti-rabbit (1:500) (Invitrogen). Slices were mounted with Vectashield solution (Vector Labs), and visualized with a Zeiss LSM Pascal confocal microscope.

Confocal data analysis of immunostaining and cell counting was performed by taking 3-D z-stacks with a 63x oil lens (Zeiss), each 202 x 202 x 60 microns in volume. To maximize accuracy of overlap determination and cell counting, cells were first identified on the green (ChR2-GFP) and red (cell-type marker) channels separately, then overlap was assessed.

For measuring the diameters of the spheres of virally-labeled cells, images containing well-isolated spheres of GFP fluorescence (n = 6 such sites) were taken using an Olympus fluorescence microscope (using 4x or 10x objective lenses). We measured the diameter of each virus sphere as follows, using ImageJ (NIH): first, we visually estimated the center of each virus sphere by examining each section through the virus sphere, and drew a randomly-oriented line through this center. (In choosing this line we did, however, avoid the cannula injection hole.) Then, we extracted the magnitudes of the fluorescence values for each pixel along this line, after performing a flat-field correction. The diameter of the spheres of GFP fluorescence was then determined as the distance between the two points at which the fluorescence fell to 20% of the peak, defined as the median of the 50 highest fluorescence values along the line. To facilitate comparison of different images for statistical purposes, we normalized each set of magnitudes to the peak, and identified the midpoint as halfway between the two points at which the fluorescence fell to 20% of the peak. For the population data (**Supplemental Fig. 4**), the normalized curves were aligned at their midpoints, and mean and standard deviation were calculated.

Western blotting. Non-human primate blood samples were collected in a Sarstedt Serum Monovette tube, and centrifuged in a Hettich Rotofix 32 Centrifuge at 2,000 RPM for 10 minutes. The serum was then transferred into a Sarstedt screw cap storage tube and then stored at -80 °C until ready for analysis. HEK cell membranes containing ChR2-GFP were prepared by transfecting 10-cm plates of HEK cells with ChR2-GFP under the CAG promoter. 3 days later, the cells from one such plate, as well as one control plate, were resuspended in PBS and centrifuged for 10 min at 2000 rpm in a benchtop centrifuge at 4^{o}C. Cell pellets were resuspended in 1 ml PBS with proteinase inhibitors (Roche), lysed in a cup sonicator for 15 seconds and centrifuged for 2 minutes at 13,000 rpm at 4^{o}C. The pelleted membranes were then resuspended in 0.5 ml Laemmli sample buffer containing SDS (Bio-Rad Inc.). For Western blotting, wells of 12% polyacrylamide gels (Bio-Rad Inc.) were loaded with 15 μl of this solution, or of a 1:5 dilution thereof. Additionally, some wells were loaded with 0.02 μL of monkey serum (a total of 15 μL, containing 1:750 diluted monkey serum), in order to assay the antibody content. After electrophoresis, proteins were transferred from the gel to a PVDF membrane (Bio-Rad

Inc.), which was then washed for 10 mins in TBS (20 mM Tris/HCl and 150 mM NaCl, pH, 7.4), blocked with 3% BSA in TBS for 2 hours, then washed and incubated with rabbit-anti-GFP antibody (1:1000, Invitrogen) or monkey serum for 2 hours at 4^{o}C while shaking. The PVDF membrane was then washed 3 times for 10 mins each, with 0.5% Tween 20 in TBS, followed with washing in TBS once, and then incubated with horseradish peroxidase (HRP)-conjugated goat-anti-rabbit or rabbit-anti-monkey secondary antibody (1:80,000, Sigma) for 2 hours. The PVDF membrane was then washed again, as described above. HRP was then imaged by adding Western Lightning Chemiluminescence Reagent Plus substrate (PerkinElmer).

REFERENCES

Aktas, O., Smorodchenko, A., Brocke, S., Infante-Duarte, C., Schulze Topphoff, U., Vogt, J., Prozorovski, T., Meier, S., Osmanova, V., Pohl, E.*, et al.* (2005). Neuronal damage in autoimmune neuroinflammation mediated by the death ligand TRAIL. Neuron *46*, 421-432.

Ayling, O.G., Harrison, T.C., Boyd, J.D., Goroshkov, A., and Murphy, T.H. (2009). Automated light-based mapping of motor cortex by photoactivation of channelrhodopsin-2 transgenic mice. Nat Methods.

Bernstein, J.G., Han, X., Henninger, M.A., Ko, E.Y., Qian, X., Franzesi, G.T., McConnell, J.P., Stern, P., Desimone, R., and Boyden, E.S. (2008). Prosthetic systems for therapeutic optical activation and silencing of genetically-targeted neurons. Proceedings - Society of Photo-Optical Instrumentation Engineers *6854*, 68540H.

Bien, C.G., Bauer, J., Deckwerth, T.L., Wiendl, H., Deckert, M., Wiestler, O.D., Schramm, J., Elger, C.E., and Lassmann, H. (2002). Destruction of neurons by cytotoxic T cells: a new pathogenic mechanism in Rasmussen's encephalitis. Ann Neurol *51*, 311-318.

Boyden, E.S., Zhang, F., Bamberg, E., Nagel, G., and Deisseroth, K. (2005). Millisecond-timescale, genetically targeted optical control of neural activity. Nat Neurosci *8*, 1263-1268.

Gratzel, M. (2001). Photoelectrochemical cells. Nature *414*, 338-344.

Honda, K. (2004). Dawn of the evolution of photoelectrochemistry. Journal of Photochemistry and Photobiology A: Chemistry *166*, 63-68.

Mitchell, J.F., Sundberg, K.A., and Reynolds, J.H. (2007). Differential attention-dependent response modulation across cell classes in macaque visual area V4. Neuron *55*, 131-141.

Murphy, K.M., Travers, P., and Walport, M. (2007). Janeway's Immunobiology, 7th edn.

Naldini, L., Blomer, U., Gallay, P., Ory, D., Mulligan, R., Gage, F.H., Verma, I.M., and Trono, D. (1996). In vivo gene delivery and stable transduction of nondividing cells by a lentiviral vector. Science *272*, 263-267.

Ridet, J.L., Malhotra, S.K., Privat, A., and Gage, F.H. (1997). Reactive astrocytes: cellular and molecular cues to biological function. Trends Neurosci *20*, 570-577.

Wang, H., Peca, J., Matsuzaki, M., Matsuzaki, K., Noguchi, J., Qiu, L., Wang, D., Zhang, F., Boyden, E., Deisseroth, K.*, et al.* (2007). High-speed mapping of synaptic connectivity using photostimulation in Channelrhodopsin-2 transgenic mice. Proc Natl Acad Sci U S A *104*, 8143-8148.

Han et al., Supplementary Figure 1

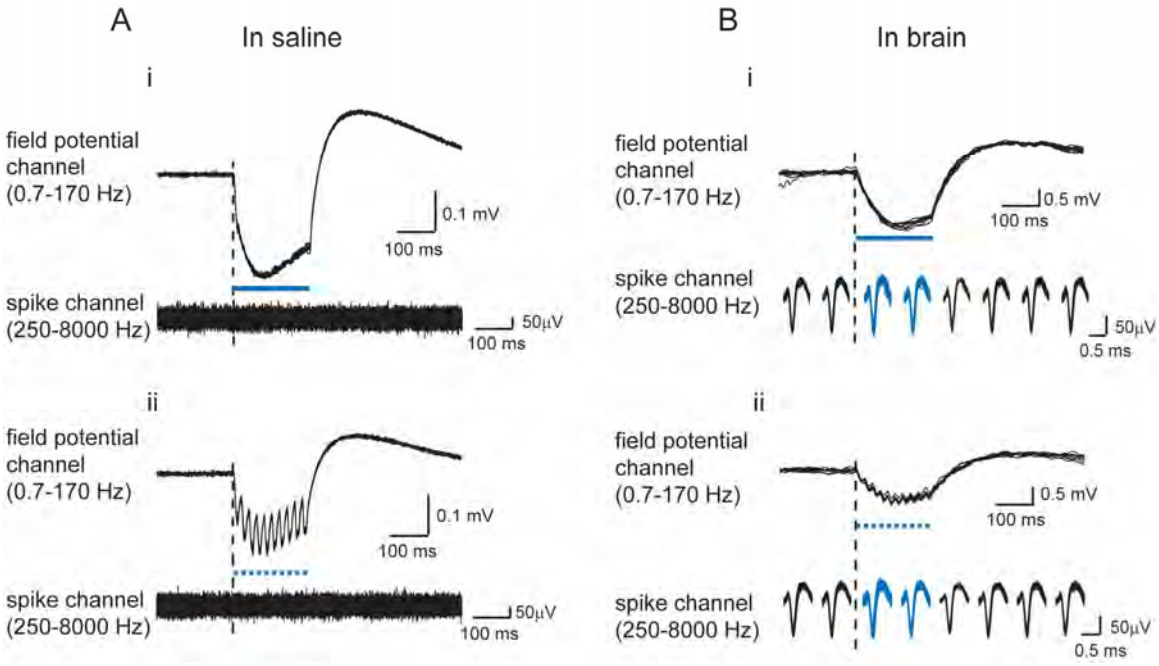

Han et al., Supplementary Figure 2

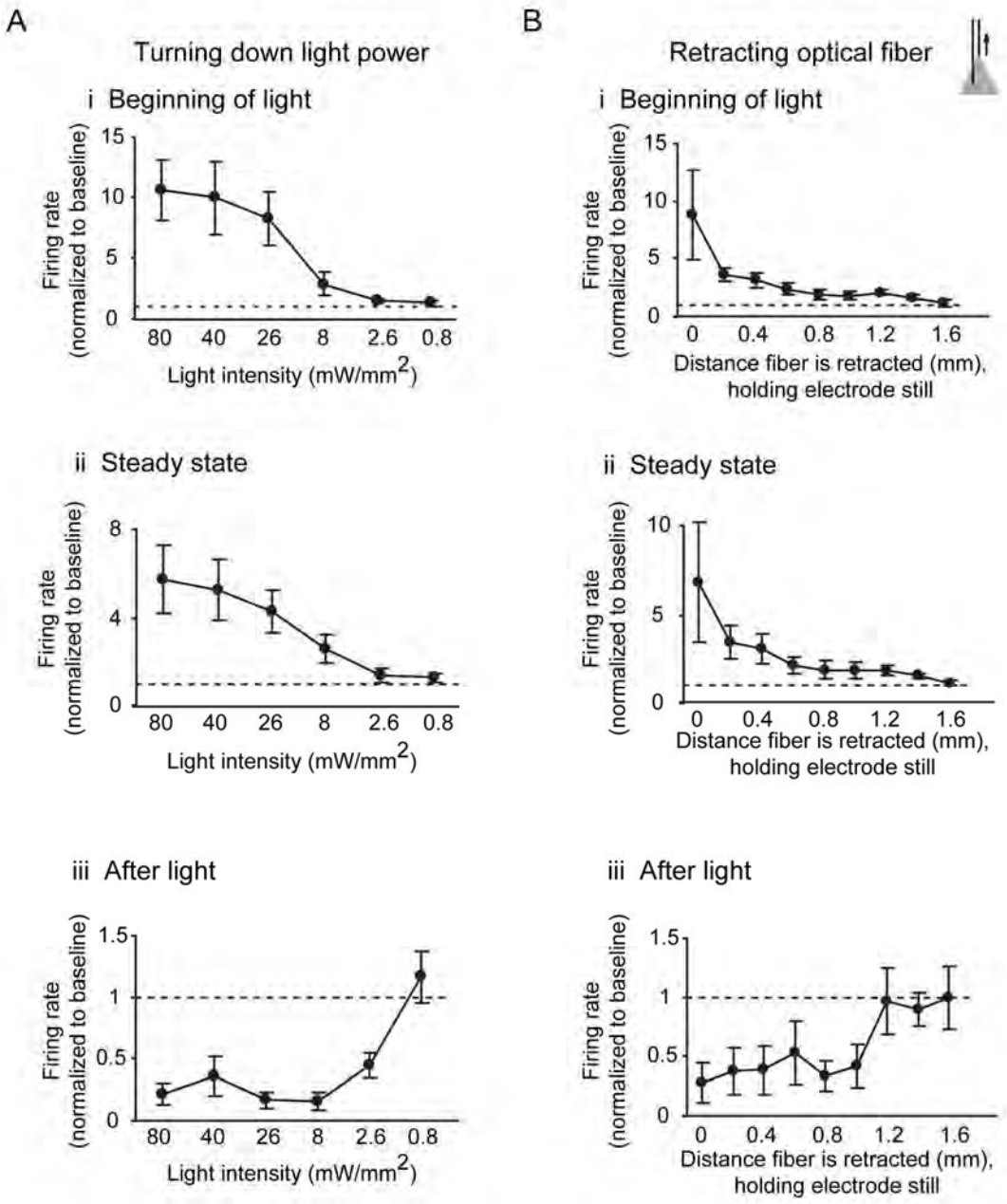

Han et al., Supplementary Figure 3

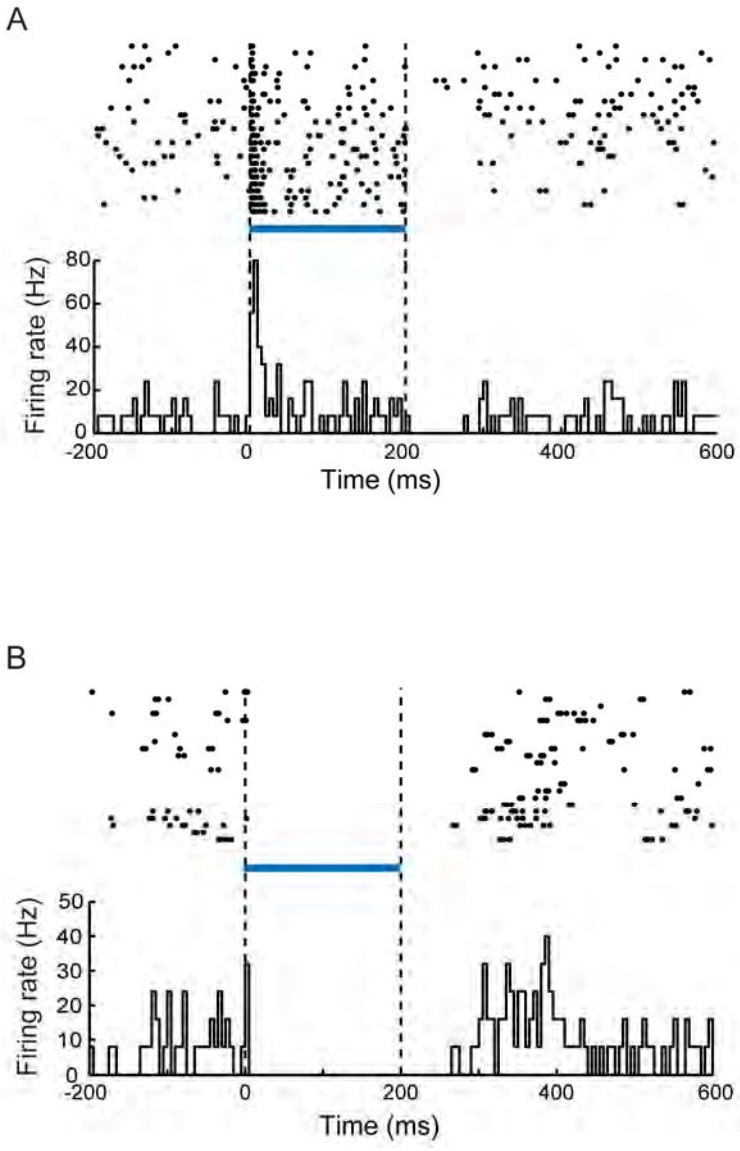

Han et al., Supplementary Figure 4

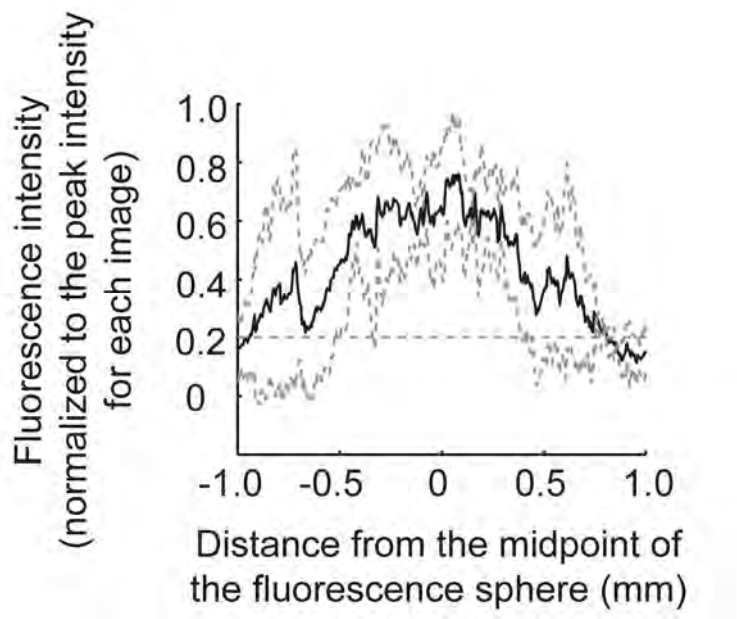

Han et al., Supplementary Figure 5

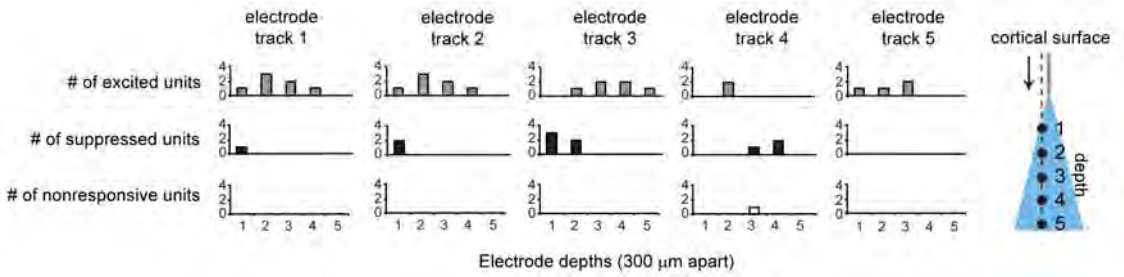

Han et al., Supplementary Figure 6